Periodical Part, Report, Published Version

Kirches, Grit; Paperin, Michael; Klein, Holger; Brockmann, Carsten; Stelzer, Kerstin

The KLIWAS Climatology for Sea Surface Temperature and Ocean Colour Fronts in the North Sea

KLIWAS Schriftenreihe

KLIWAS

Klima · Wasser · Schifffahrt

The KLIWAS Climatology for
Sea Surface Temperature and
Ocean Colour Fronts in the North Sea

Part A: Methods, Data, and Algorithms

Koblenz, im Oktober 2013

BROCKMANN
CONSULT GMBH

BSH

BUNDESAMT FÜR
SEESCHIFFFAHRT
UND
HYDROGRAPHIE

Fronts
Recognition and analysis of time series
derived from satellite data

KLIWAS Schriftenreihe
KLIWAS-23/2013

**The KLIWAS Climatology for
Sea Surface Temperature and
Ocean Colour Fronts in the North Sea**

Part A: Methods, Data, and Algorithms

Authors:

Grit Kirches [1]
Michael Paperin [1]
Holger Klein [2]
Carsten Brockmann [1]
Kerstin Stelzer [1]

[1] Brockmann Consult GmbH
[2] Federal Maritime and
   Hydrographic Agency

Brockmann Consult GmbH, Max-Planck-Straße 2, 21502 Geesthacht,
Germany

Federal Maritime and Hydrographic Agency, Bernhard-Nocht-Straße 78, 20359 Hamburg,
Germany

CLIMATOLOGY

of SST and Water Colours Fronts in the North Sea
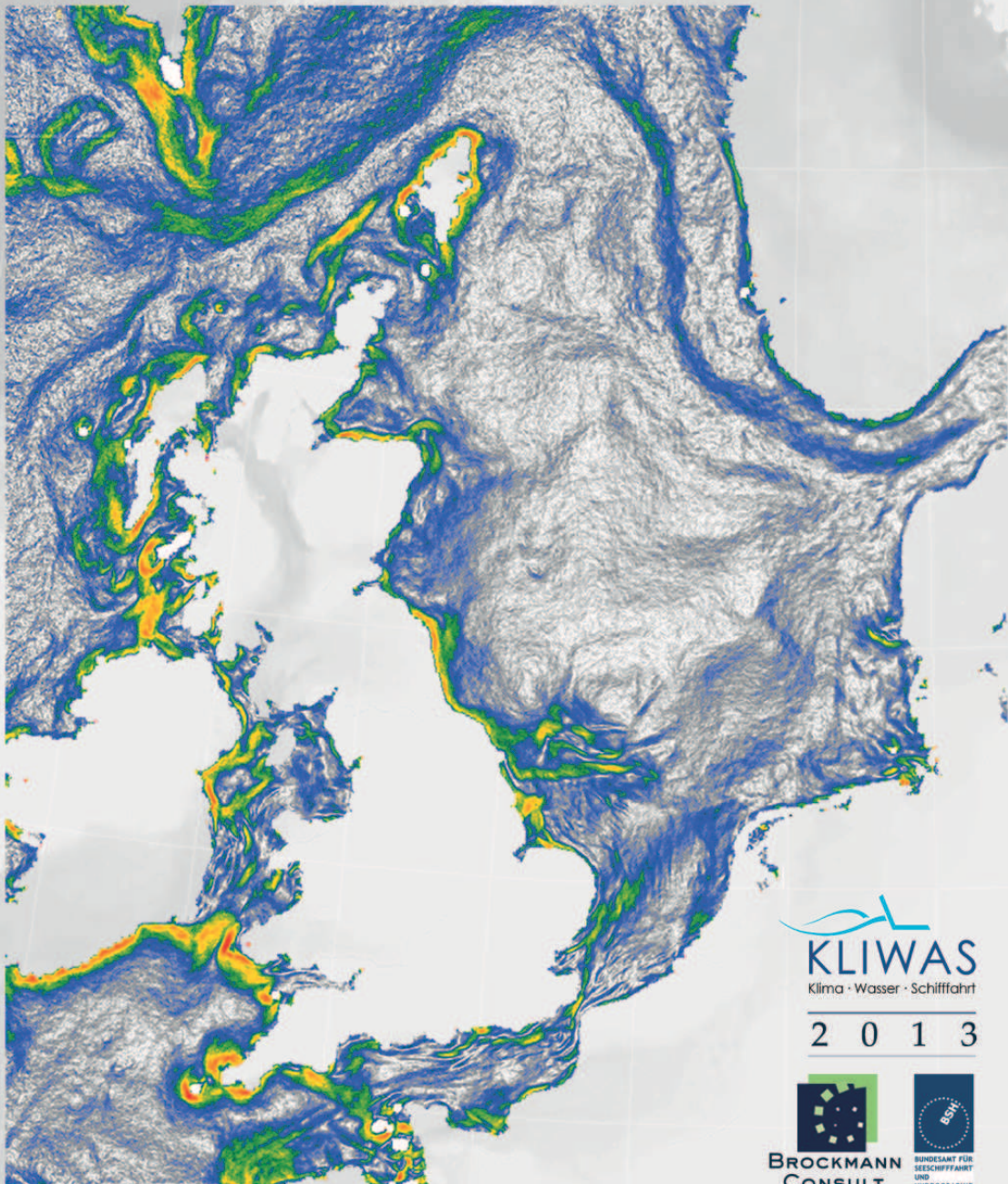
KLIWAS
Klima · Wasser · Schifffahrt

2 0 1 3

BROCKMANN CONSULT

BSH
BUNDESAMT FÜR
SEESCHIFFFAHRT
UND
HYDROGRAPHIE

Page   Chapter

Contents

List of figures

List of tables

List of Abbreviations

AATSR	Advanced Along-Track Scanning Radiometer
	https://earth.esa.int/web/guest/missions/esa-operational-eo-missions/envisat/instruments/aatsr
AVHRR	Advanced Very High Resolution Radiometer
	https://earth.esa.int/web/guest/missions/3rd-party-missions/current-missions/noaa-avhrr
BC	Brockmann Consult
BSH	Bundesamt für Seeschifffahrt und Hydrographie
C2R	Case 2 Regional
DWD	Deutscher Wetterdienst
E	East
ECHAM	atmospheric general circulation model, developed at the Max Planck Institute for Meteorology
EEZ	Exclusive Economic Zone
EO	Earth Observation
ETOPO1	1 arc-minute global relief model of Earth's surface that integrates land topography and ocean bathymetry
EUMETCast	EUMETSAT's Multicast Distribution System
EUMETSAT	European Organisation for the Exploitation of Meteorological Satellites
	http://www.eumetsat.int/website/home/index.html
GAC	Global Area Coverage
GES	Good Environmental Status
GHRSST	The Group for High Resolution SST www.ghrsst.org
GSST	Gridded Sea Surface Temperature
HDF	Hierarchical Data Format
HIRHAM	regional atmospheric climate model
HRPT	High-Resolution Picture Transmission
ICDC	Integrated Climate Service Center
ICES	International Council for the Exploration of the Sea
IPSLCM	Institut Pierre-Simon Laplace climate model
KD490	diffuse attenuation coefficient at 490 nm
KLIWAS	Impacts of climate change on waterways and navigation - Searching for options of adaptation
LAC	Local Area Coverage
MERIS	MEdium Resolution Imaging Spectrometer
	https://earth.esa.int/web/guest/missions/esa-operational-eo-missions/envisat/instruments/meris
MetOp	Meteorological Operational Satellite
	http://www.eumetsat.int/website/home/Satellites/CurrentSatellites/Metop/index.html
MPI-OM	Max Planck Institute ocean model
MODIS	Moderate Resolution Imaging Spectroradiometer

	http://modis.gsfc.nasa.gov/data/	
MSLP	Mean Sea Level Pressure	
N	North	
NaN	Not a Number	
NASA	National Aeronautics and Space Administration	
NCEP	National Centers for Environmental Prediction	
	http://www.ncep.noaa.gov/	
NCAR	National Center for Atmospheric Research	
	http://ncar.ucar.edu/	
NE	Northeast	
NGDC	NOAA's National Geophysical Data Center	
	www.ngdc.noaa.gov/	
NOAA	National Oceanic and Atmospheric Administration	
	www.noaa.gov/	
NW	Northwest	
OC	Ocean Colour	
OLCI	Ocean and Land Colour Instrument	
	http://www.esa.int/Our_Activities/Observing_the_Earth/Copernicus/Sentinel-3	
RACMO	Regional Atmospheric Climate Model	
RCM	Regional climate model	
REMO	Regional Model suitable for climate modelling and weather forecast	
RGB	Red Green Blue, additive color space based on the RGB color model	
RPF	River Plume Front	
RR	Reduced Resolution	
S	South	
SE	Southeast	
SEADAS	SeaWiFS Data Analysis System	
	http://oceancolor.gsfc.nasa.gov/	
SIED	Single-Image Edge Detection	
SLSTR	Sea and Land Surface Temperature Radiometer	
	http://atsrsensors.org/slstr.htm	
SST	Sea Surface Temperature	
SW	Southwest	
TMF	Tidal Mixing Front	
TSM	Total Suspended Matter	
TOA	Top of Atmosphere	
UHR	Ultra-High Resolution	
UK	United Kingdom	
UTM	Universal Transverse Mercator projected coordinate system	
W	West	
WGS	World Geodetic System	
YS	Yellow Substance	

1   Abstract

The KLIWAS climatology of sea surface temperature (SST) and ocean colour (OC) fronts in the North Sea was established by a co-operation of the Federal Maritime and Hydrographic Agency (BSH) and Brockmann Consult (BC) in order to generate a reliable reference data set for the assessment of changes in frontal position, gradients, and seasonal variability due to climate change on the basis satellite data.

Frontal zones are relative sharp boundaries between different water masses and can be identified by feature extraction and classification of satellite data from different sensors providing information about the SST and OC i.e. chlorophyll or suspended matter concentration. While frontal zones of thermal fronts can be identified directly from SST, water quality parameters such as chlorophyll concentration can be a proxy for a frontal zone, but not every strong OC gradient is mandatory an oceanic front. More than two decades of satellite data have been analysed for this climatology referring to type and location of frontal zones, horizontal scales (e.g. gradients perpendicular to the front), and sensor characteristics like spatial resolution and noise.

This report consists of three parts:

Part A (this document) describes background, methods, data, the algorithms, and the data access via ftp. The data are freely available for everyone.

Part B presents a selection of SST products, and

Part C presents a selection of OC products.

2   Climate Change, Oceanic Fronts and their particular Importance for KLIWAS: An Introduction

In our daily life we experience fronts as a directly sensible phenomenon by the passage of meteorological fronts which separates different air masses: The weather changes and we feel a change of wind speed and direction, temperature, precipitation and/or cloudiness. Comparable phenomena also exist in the ocean: Oceanic fronts are distinct boundaries between water bodies with different properties. They are associated with horizontal and vertical transports and have a great impact on local dynamics, ecology, marine economy and on the ocean's uptake of CO_2. Climate related changes in the North Sea will inevitably have an impact on the location of fronts and the strength of their gradients. These changes and their consequences have to be assessed within the marine part of KLIWAS.

Due to a worldwide meteorological monitoring network running for many decades we are well informed about the dynamics and impacts of atmospheric fronts. However, our knowledge about oceanic fronts is still limited. Now, after more than two decades of satellite-borne remote sensing of the oceans, we have the possibility to compile a reliable climatology of frontal positions and gradients by analysing long time-series to set-up a reference data set as a basis for the assessment of possible changes in the oceans due to climate change. This climatology of North Sea fronts is a valuable addition to the new KLIWAS North Sea Climatology for oceanic and atmospheric in-situ data which was developed in a close co-operation of the Federal Maritime and Hydrographic Agency (BSH), the German Meteorological Service (DWD) and the Integrated Climate Data Center (ICDC) of the University Hamburg[1]. Both climatologies complement each other and provide together a solid set of reference data.

Oceanic fronts are important dynamic meso-scale structures which have a significant impact on local dynamics, biology, ecology and – due to their ability to transport CO_2 into greater depths – also on climate. The coastal areas of the North Sea, especially the German, Dutch and UK coasts, are dominated by river plume fronts (RPF) with strong salinity and turbidity gradients between the fresh water run-off of the big continental rivers and the coastal North Sea waters. Roughly following the 30 m isobath, tidal mixing fronts (TMF) separate the seasonally (about end of March until September) thermal stratified parts of the deeper North Sea from the shallower coastal areas which are vertically mixed due to wind and tidal mixing. Other frontal structures are caused, e.g., by the intrusion of the brackish Baltic outflow into the

---

[1] http://icdc.zmaw.de/knsc.html

Skagerrak area and by topographically induced up- or down-welling above the Norwegian Trench. At the northern boundary of the North Sea, Atlantic Water, the mixed Scottish Shelf and North Sea waters are separated by fronts which give valuable indications on the dynamics of exchange processes due to their spatial structure and eddy displacements.

Frontal structures are also characterised by strong biological activity and the adjacent stratified regions play a key role in marine ecosystems. They affect ecosystem components at all levels, directly or through cascading across the food-web (ICES 2006). Fronts, with their strong vertical velocities, can lift nutrients into the euphotic layer and enhance the productivity of the ocean. They can also increase light exposure by modulating the rate at which phytoplankton is mixed below the euphotic layer (Ferrari 2011). This high biological activity, stimulated by both high inputs and efficient use of nutrients, mediates the drawdown of CO_2 from the atmosphere and its subsequent export to subsurface layers. The ultimate outflow of such CO_2-enriched subsurface waters to the open deep ocean constitutes the so-called 'shelf sea pump', a mechanism which transfers CO_2 to the open ocean and which is thought to substantially contribute to the global ocean's uptake of atmospheric CO_2. The North Sea acts as a sink for CO_2 over wide areas throughout the entire year except during the summer months in southern parts of this region. More than 90% of the CO_2 taken up by the North Sea from atmosphere is exported into the North Atlantic. Extrapolating the North Sea's CO_2 uptake over all shelf sea areas worldwide results into a global net uptake of 20% of all anthropogenic CO_2 by the ocean due to shelf sea pumping (Thomas et al. 2004).

Climate related changes in the North Sea and in the adjacent North Atlantic will impact atmospheric and oceanic circulation patterns, tides, sea level, precipitation patterns and intensity, salinity and continental river run-off volumes. These changes in turn will have an influence on the position, strength and dynamic of oceanic fronts and thereby on biology, ecology and the intensity of shelf sea pumping. ICES (2006) stated: 'an understanding of fish response to climate compatible with process understanding requires that meso-scale oceanic features can be detected and tracked over long periods of time.' Such an operational monitoring is possible only by the use of satellite earth observation (EO) data and with algorithms being able to detect different types of fronts automatically. To assess alterations caused by climate change, there is an urgent need for reliable information about positions and intensities of fronts and their seasonal and wind dependent variability. Ferrari (2011) asked: 'Given the importance of frontal physics and biogeochemistry, how are we going to make substantial progress in understanding and quantifying the effect of fronts on the global climate system?'

The KLIWAS climatology of North Sea fronts, realised by a co-operation of Brockmann Consult and BSH, is a contribution to answer these questions. The new method for front detection called GRADHIST is basing on the combination and

refinement of two existing stand-alone algorithms added by a merging module which combines the special skills of the individual algorithms. GRADHIST is able to detect frontal positions and gradient strength in satellite data and can process big data volumes automatically. The focus lies on sea surface temperature (SST) and so-called ocean colour (OC) data which allow the determination of chlorophyll, turbidity, transparency and yellow substance, parameter which are well suited to distinguish different water bodies in the ocean.
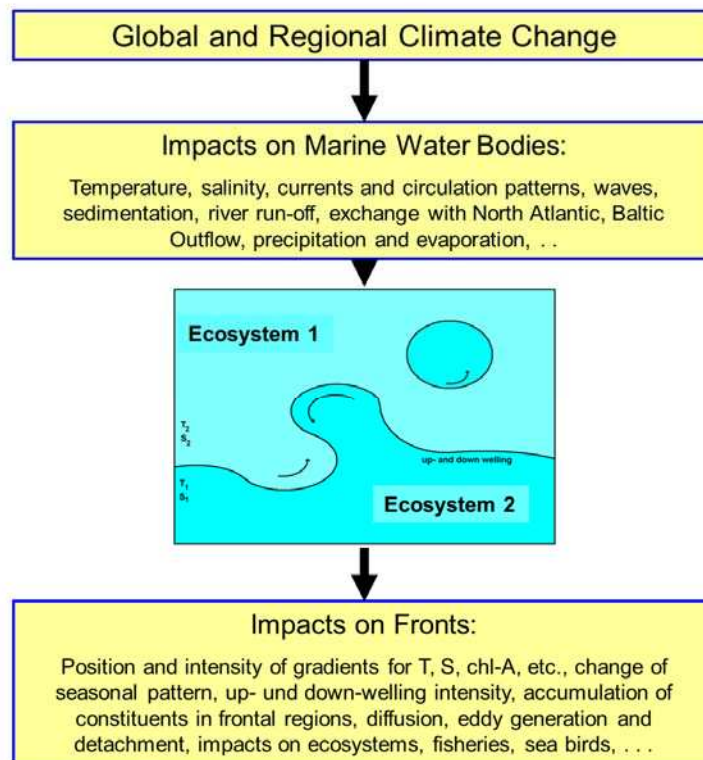
Fig. 1: Impact of climate change on fronts and ecosystems

The importance of oceanic fronts for KLIWAS is given by their dynamical aspects, especially their vertical transports of nutrients, plankton and anthropogenic CO_2 (self sea pumping). Due to their impact on ecology fronts are important for marine economy like fisheries and aqua culture. Therefore, many areas in the North Sea dominated by fronts are designated protected areas, e.g., the Frisian Front along the Dutch coast. Besides taking an inventory of frontal positions, their properties and their natural variability, it is important to observe and to assess future changes of frontal systems. The new detection method also enables an operational monitoring of front positions and gradients as demanded by ICES (2006). Further on, fronts as protected areas play an important role in marine spatial planning and have therefore a direct impact on the economic use of the German Exclusive Economic Zone (EEZ). The operational use of the new method may also help in assuring the so-called 'Good

Environmental Status' (GES) as required by the European Marine Strategy Framework Directive (The European Commission, 2010).

3   Algorithm Description

3.1   Approaches to feature detection

The advent of remote sensing from satellites has enabled global monitoring of oceanic fronts from space. The first parameter used for this purpose was the sea surface temperature (SST). SST fronts are caused by different physical processes like convergence of different water masses, river run-off, or up- and down-welling etc. These SST gradient zones can be detected in SST images by objective methods.

Two approaches became widely accepted: the gradient method, e.g. the Canny edge detector, mainly due to its simplicity and the histogram method, due to its robustness and comprehensive worldwide validation (Canny 1986, Cayula and Cornillon, 1992). Other methods have been developed as well, notably the cluster-shadow method, wavelet methods and classification of water masses (Belkin and O'Reilly, 2009).

Gradient-Algorithm

The search-based methods detect edges by first computing a measure of edge strength, usually a first-order derivative expression such as the gradient magnitude, and then searching for local directional maxima of the gradient magnitude using a computed estimate of the local orientation of the edge, usually the gradient direction (Canny 1986, Jähne 2005). Different published edge detection methods mainly differ in the types of applied smoothing filters, in the types of the filter used for computing of the gradient and by the way to determine the edge strength.

Histogram-Algorithm

Histograms as graphical representation of the probability density function of the underlying variable can be used for edge detection as well. Histogram algorithms are search-based methods that detect edges by testing if more than one population (in this case water mass) is present in the area under consideration. Edge detection methods mainly differ in their requirements on noise removal and the way to decide if the hypothesis of more than one population can be accepted (Cayula and Cornillon 1992, 1995 and 1996).

3.2   Theoretical Algorithm Description

Miller (2009), Shimada et al. (2005), Belkin and O'Reilly (2009), Vazquez et al. (1999) and others have demonstrated the general feasibility of detecting SST and OC fronts in satellite data. In their studies, the automatic detection of fronts in large data volumes is done either by a gradient algorithm, which exploits spatial gradients within a satellite image, or a histogram algorithm, which works on the frequency distribution of the values within image subsets. The strength of the gradient algorithms is that they enable the detection of any front regardless of its strength, as

shown by Castelao (2006) and by Belkin and O'Reilly (2009). However, gradient algorithms are not able to recognise and discard false fronts caused by noise. On the other hand, histogram algorithms are able to detect weak fronts in the presence of high background noise as shown by Cayula and Cornillon (1992, 1995, 1996), Diehl et al. (2002) and, Ullman and Cornillon (1999, 2000, 2001). In the present study, a new approach was developed which combines and modifies the gradient algorithm of Canny (1986) and the histogram algorithm of Cayula and Cornillon (1992) in order to improve the front detection ability. It was also found that a proper pre-processing of the data is important in order to have a good detection quality for fronts. The pre-processing includes mainly cloud filtering and noise reduction. We call this new approach GRADHIST. The flowchart in Fig. 2 outlines the overall processing chain of GRADHIST which includes three steps: pre-processing, the application of the modified gradient and histogram algorithms and the matching module.
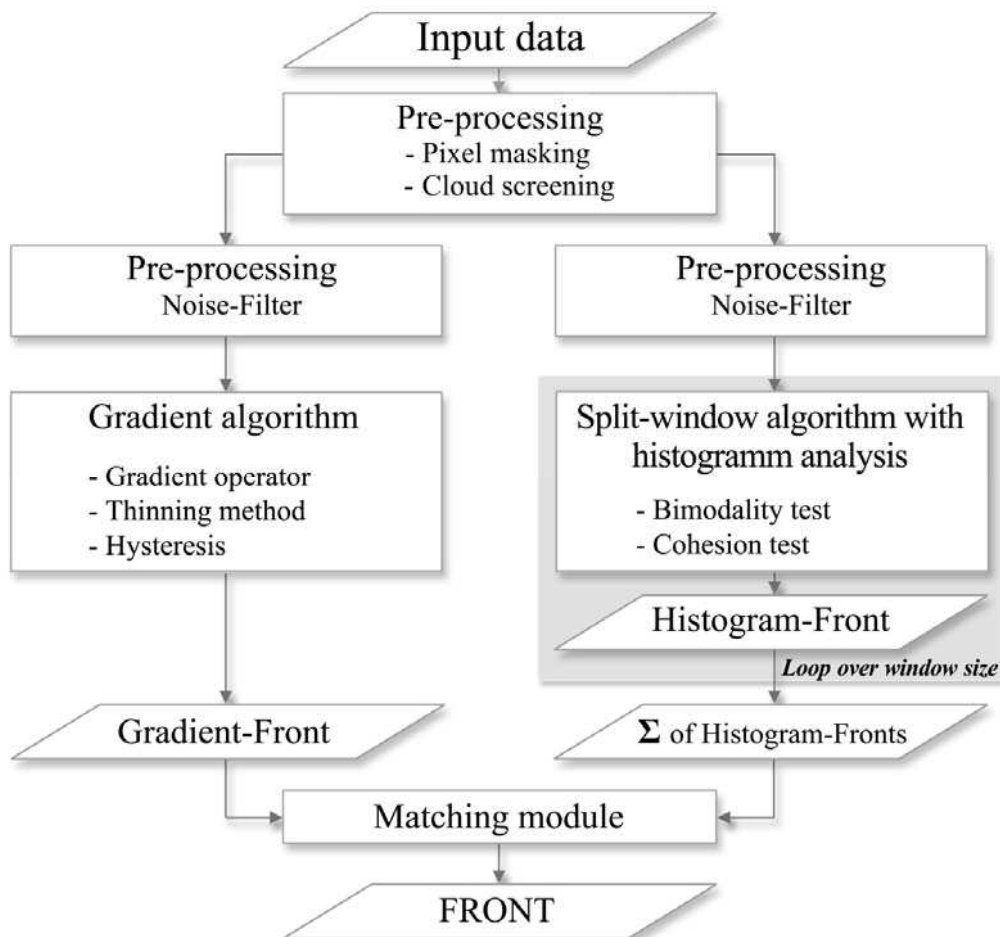

Fig. 2: Flowchart of front detection algorithm

3.2.1 Pre-processing

Frequent cloud cover over the North Sea is the main factor which limits the availability of suitable data. It is important that clouds are accurately identified in order to properly retrieve SST and OC parameters. The cloud mask is an integral part of standard level 2 products, but its quality varies between different sensors and their cloud detection algorithms. The AATSR[2] cloud mask for example can be used without any modifications, whereas the cloud mask of the MERIS and MODIS is not precise enough for the purpose of front detection (residual clouds are detected as fronts). In this case, the cloud detection has to be improved for both sensors by the application of additional algorithms. The AVHRR data provided by the BSH already include a manually improved cloud mask. Because the edges of clouds are often not well defined, a cloud buffer or border has been additionally introduced. The following figure (Fig. 3) shows the resulting cloud, cloud shadow and land masks in a MERIS image.
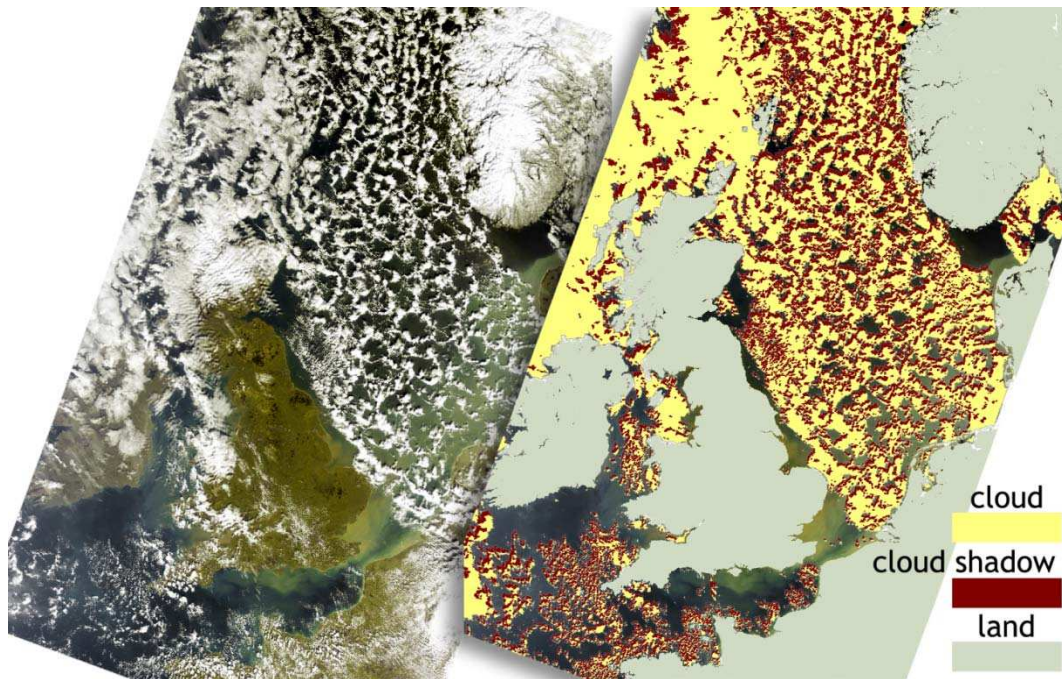
Fig. 3: a) RGB; b) corresponding cloud and land mask for MERIS RR 2012.02.19, Orbit: 52163

Sensor electronics, spectral resolution, digital quantification and other effects cause noise which can hamper image processing algorithms and especially edge detection algorithms (Fisher et al. 2003). Hence a high degree of noise reduction is necessary before applying the gradient and histogram front detection algorithms. Due to its edge-preserving nature a median noise filter was used in the histogram algorithm while a Gaussian noise filter is better suited to the gradient algorithm because it removes small scale details.

---

[2] For different sensor types see Table 1 in chapter 4!

In order to increase the number of useable image pixels, small gaps of 1-2 pixels due to small clouds or otherwise missing data were filled with the average value of the neighbouring cloud-free water pixels. Furthermore, the OC parameter distribution is approximately lognormal and therefore the OC parameter data were converted to logarithmic values before processing (Campbell 1995, Gregg and Casey 2004).

3.2.2 Front Detection

The first part of the front detection is based on the Canny edge detection algorithm which belongs to the group of gradient algorithms (Canny 1986, Castelao 2006). The application of the edge detection algorithm is based on a structured 4-step procedure involving noise reduction, calculation of the gradient, non-maximum suppression, and tracing edges through the image by hysteresis thresholding. The second part of the front detection works on the principle of the Single-Image Edge Detection algorithm (SIED) according to Cayula and Cornillon (1992, 1995 and 1996) which is a widely used histogram algorithm. The application of this edge detection method includes histogram analysis, the application of a cohesion algorithm using a fixed investigation window size and a contour-following algorithm. In GRADHIST, we used all steps except the contour filling. In the final step of the GRADHIST processing chain the resulting fronts of both algorithms are merged into a final front map (Kirches et al. 2013).

The SST field from a scene of NOAA 17 AVHRR sensor and its SST fronts identified by GRADHIST are shown in Fig. 4. The advantages of GRADHIST are the equally good detection of strong and weak fronts, the determination of the gradient magnitude as well as the gradient direction, and the ability to process large data volumes fully automatically.
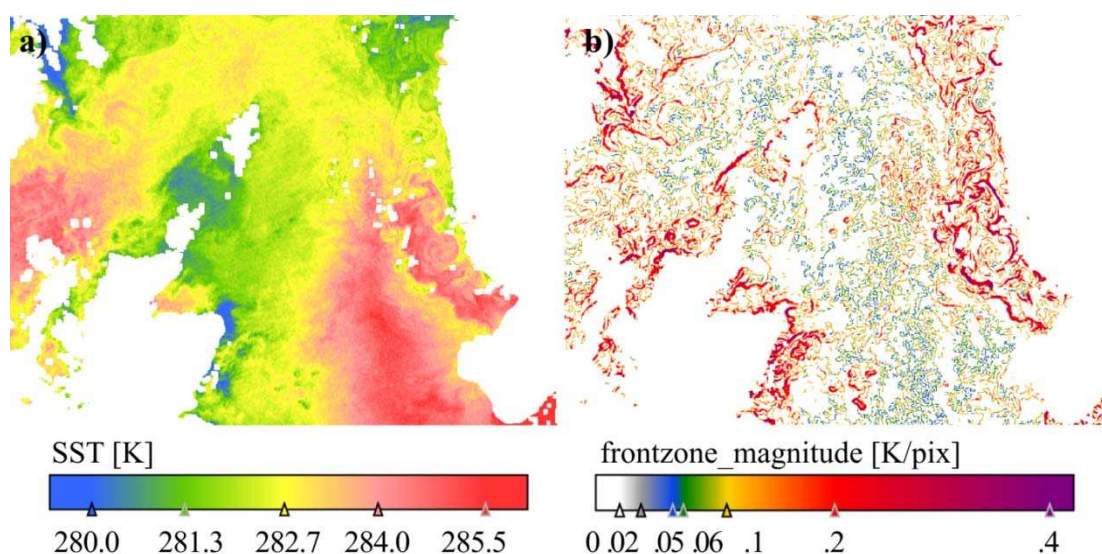

Fig. 4: SST field and SST frontal zones in the northern part of the North Sea: fronts identified by GRADHIST (AVHRR of NOAA 17)

4 Description of input and output products

For the North Sea climatology it was necessary to process very large data volumes. The proper processing of the EO data archive was done for SST and OC parameter with different sensor data which are summarized in see Table 1.

Table 1: Data sets included into the climatology

Parameter	Sensor	Satellite	Time Period	Units
Sea Surface Temperature	AATSR	ENVISAT	2002 - 2011	K
Sea Surface Temperature	MODIS	AQUA	2003 - 2011	K
Sea Surface Temperature	AVHRR	NOAA & MetOp	1990 -2011	K
Chlorophyll	MERIS	ENVISAT	2002 - 2010	mg/m³
Total Suspended Matter	MERIS	ENVISAT	2002 - 2010	g/m³
Yellow Substance Absorption	MERIS	ENVISAT	2002 - 2010	1/m
Turbidity	MERIS	ENVISAT	2002 - 2010	1/m

4.1 SST and Ocean Colour Input Data

Input data for the front detection algorithms are pre-processed data, i.e. they are geo-corrected and cloud mask, land mask and possible "NaN" masks are applied. The cloud mask is an integral part of standard level 2 products, but the quality varies between the different sensors. Therefore additional algorithms are used to improve the cloud detection.

AATSR SST:

The AATSR Level 2 Gridded Sea Surface Temperature (GSST) product is a full spatial resolution (approximately 1km by 1km) product. Pixel information is formed by a mixture of geophysical product, surface brightness temperature/radiance and TOA[3] brightness temperature/radiance in the case of an unclassified pixel (Scarpino et al. 2009, RAL, 2007)).

---

[3] Top of Atmosphere

MODIS SST:

The Level-2 product is built from a corresponding Level-1A product. The main data contents of the product are the geophysical values for each pixel, derived from the Level-1A raw radiance counts by applying the sensor calibration, atmospheric corrections, and bio-optical algorithms. Each Level-2 product corresponds exactly in geographical coverage (scan-line and pixel extent) considering its parent Level-1A product and is stored in one physical HDF-file (Ocean Color 2009). The software SEADAS (SeaWiFS Data Analysis System) developed and provided by NASA can be used for processing individually defined Level-2 products. So the required MODIS Level-2 product for the front analysis contains 6 geophysical values derived for each pixel: the TOA reflectance of band 2135 nm, the brightness temperature of band 8.8Mm and 11µm, the SST, the chlorophyll-a concentration and the KD490. In addition, 32 flags are associated with each pixel indicating if any of the applied algorithms failed or warning conditions occurred for that pixel.

For the SST retrieval the standard MODIS 11µm SST algorithm is chosen, which uses the 11 and 12 micron channels.

AVHRR SST BSH:

Since 1990 the BSH has been receiving and processing AVHRR-data from the polar orbiter NOAA-satellites and since September 2009 in addition data from the European weather satellite MetOp by EUMETCast. BSH generates daily marine products including North Sea SST. The BSH data products available include the SST-values with a no-data value for invalid pixels on a pre-defined grid.

MERIS OC:

The MERIS Level-2 product is built from a corresponding Level-1b product. The main data contents of the product are the geophysical values for each pixel, derived from the Level-1B radiances by applying the radiometric correction, atmospheric corrections, and bio-optical algorithms. The OC retrieval algorithm used for the front detection is the Case 2 Regional algorithm (C2R). It performs an atmospheric correction above water and derives the ocean bio-optical parameters from the resulting water leaving reflectance. This algorithm is valid for all water types, including yellow substance dominated and waters with excessive back-scattering (Doerffer and Schiller 2008). In addition, flags are also associated with each pixel indicating if any algorithm failures or warning conditions occurred for that pixel such as high glint, aerosol as well as indicating the type of water.

4.2 Statistical Front Product

4.2.1 North Sea Blank

After the algorithm has been validated and tested the EO data listed in Table 1 have been processed. All input data are collocated on a spatial grid that covers the North Sea and part of the North East Atlantic. After computation of the gradient magnitude and gradient direction, a set of statistical measures was computed for SST and OC front products. All input data with the exception of the AVHRR data are collocated on a predefined subset with the following properties:

- horizontal: 0 - 1273 pixel;
- vertical: 0 - 1337 pixel;
- size: 1273 x 1337 = 1702001;
- scale: 1 km/pixel;
- projection: UTM Zone 31 WGS 1984.

The AVHRR data was delivered on other subset with the following properties: horizontal 1100 pixel; vertical 1000 pixel; size 1100000 pixel; scale ~1 km/pixel; projection Mercator. To facilitate comparison the results of the temporal statistics for the AVHRR sensor have been collocated on our predefined subset.

4.2.2 Predefined Bands in Statistical Front Products – SST & OC

The ocean bathymetry created by NOAA's National Geophysical Data Center (NGDC) is available as static information layer (Amante and Eakins, 2009). Furthermore, a static land/water mask has been applied to all input products which was derived from the bathymetry data set.
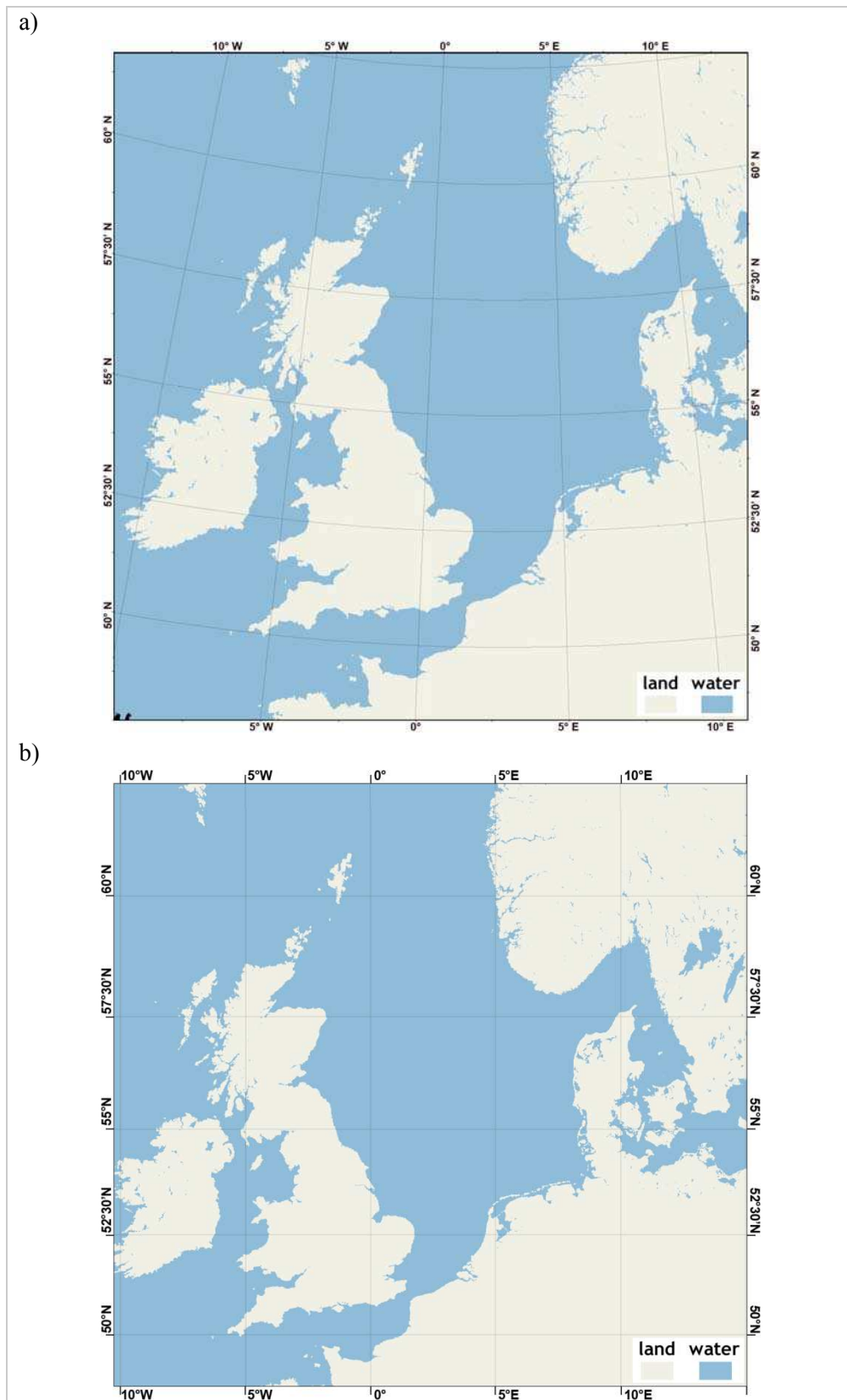
Fig. 5: Land water mask of the North Sea (data taken from the ETOPO1 Ice Surface – Amante and Eakins (2009) (a) subset for AATSR, MODIS and MERIS, (b) subset for AVHRR)
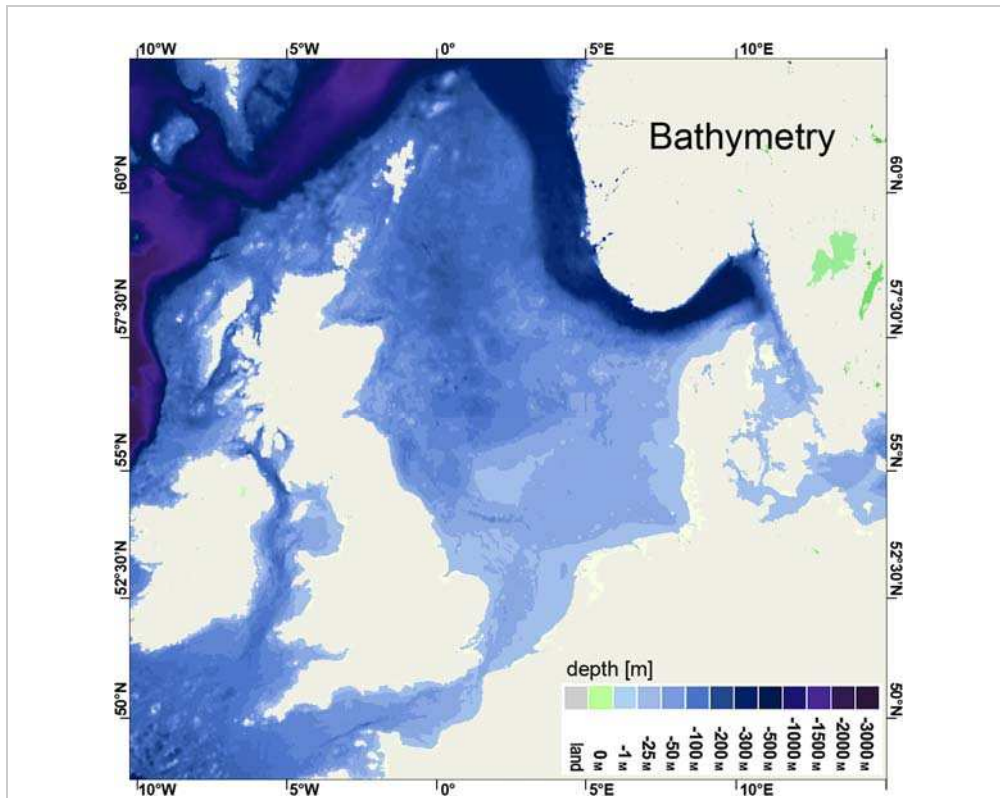
Fig. 6: Bathymetry of the North Sea (data taken from the ETOPO1 Ice Surface - Amante and Eakins, 2009)

4.2.3 Statistical Front Products – SST and OC

The following section and Equations 1 - 4 provide an overview and a definition on the measures using the example of SST. The first parameter is the mean of SST gradient magnitude for frontal zone over a defined time interval per pixel:

$$\overline{|\nabla SST|} = \frac{\sum_t^{N_{front\_obs}} |\nabla SST|_t}{N_{front\_obs}} \qquad (1)$$

with N_{fronts_obs} the number of front observations over a defined time interval per pixel. The second measure is the magnitude of mean SST parameter gradient vector for frontal zone over a defined time interval per pixel:

$$|\overline{\nabla SST}| = \left| \frac{\sum_t^{N_{front\_obs}} \nabla SST_t}{N_{front\_obs}} \right| \qquad (2)$$

The direction of mean SST parameter gradient vector for frontal zone over a defined time interval per pixel is defined as:

$$\text{Direction of } \overline{\nabla SST} = \frac{\sum_t^{N_{front\_obs}} \nabla SST_t}{N_{front\_obs}} \qquad (3)$$

One of the most important parameters is the front probability over a defined time interval per pixel

$$\text{Probability}_{front} = \frac{N_{front_{obs}}}{N_{SST}} \qquad (4)$$

with N_{SST} the number of SST observations per pixel over a defined time interval, i.e. reference period. It can therefore provide reliable information about the probability for observing a SST or OC front at this location. GRADHIST provides the possibility to derive not only the mean magnitudes but also the gradient vectors for a frontal zone. For regions which show a prevailing direction of the gradient vectors both measures are nearly in the same order of magnitude, i.e., the fronts have a high directional persistence. If the magnitude of mean SST/OC gradient vector is apparently smaller than the mean of SST/OC gradient magnitude, the frontal zone is characterized by a high directional variability. Fig. 7 shows the distribution of the gradient vectors as well as the resulting mean gradient vector for two selected locations marked by pins. Furthermore, the histogram of the direction of the SST front gradient vectors is also shown.
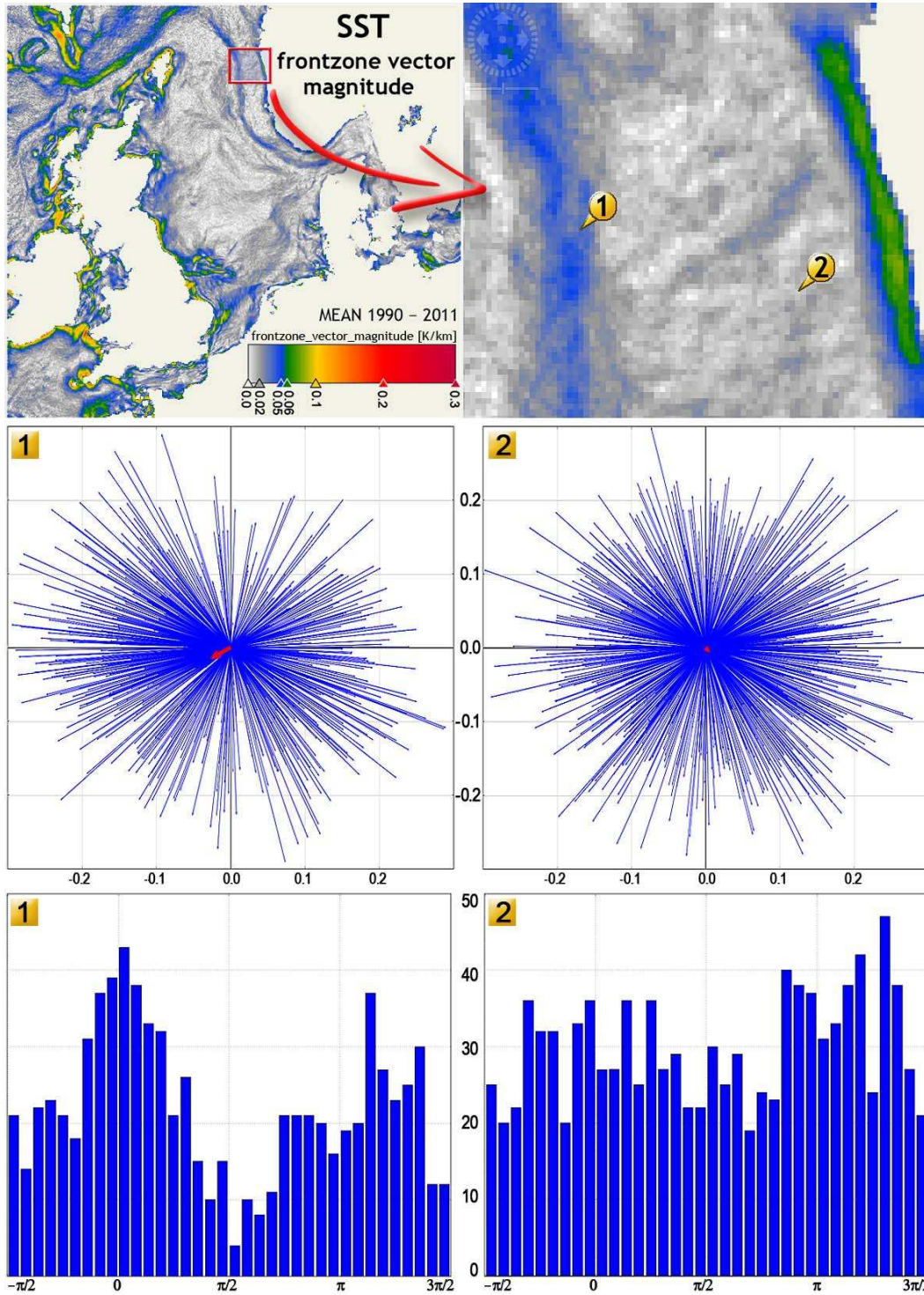
Fig. 7: Distribution of the SST front gradient vectors and histogram of the direction of the SST front gradient vectors for two selected locations (p1: 60.47676°N, 3.349396°E; p2: 60.31009°N, 4.313275°E) and retrieved from the AVHRR data 1990 – 2011

For each SST and OC parameter a total of eight values have been determined per pixel (see Table 2). As mentioned before, the statistical measures have been calculated over certain time periods. Thus, yearly and seasonal mean measures have been retrieved and in the case of SST from the AVHRR image the monthly mean measure has been retrieved respectively.

Table 2: Values supplied for the statistical SST/OC front product

No.	Value	Description
1	LandWater	Land water mask
2	depth_ETOPO1_ice	Land topography and ocean bathymetry
3	parameter_count	Number of observations
4	frontzone_count	Number of observations of frontal zone over a defined time interval
5	frontzone_propability	Probability of a front observation
6	frontzone_magnitude_total	Mean gradient magnitude for frontal zone
7	frontzone_vector_magnitude	Magnitude of mean gradient vector for frontal zone
8	frontzone_vector_direction	Direction of gradient vector for frontal zone

5 The impact of the local wind field on SST fronts in the German Bight

Beside the annual, seasonal, and monthly climatological SST products presented in **Part B** of this report, also the dependency of frontal position and gradient strength from prevailing wind directions was analysed. Especially for river plume fronts in the German Bight it is known from in-situ and EO data, that the local wind field has an impact on front position and gradient strength. Therefore – as a first approach – the procedure of Jenkinson and Collision (1977) for an objective determination of the 'Lamb Weather Types'[4] was applied. This procedure allows a classification of daily large-scale weather situations basing on mean sea level pressure (MSLP) data only. This procedure was applied to a North Sea sub-sample of daily MSLP NCEP/NCAR fields[5]. It provides indices for wind and vorticity which are representative for the whole North Sea region. Empirical relations between these indices determine the circulation type (e.g. cyclonic, anti-cyclonic, north-west, etc.) and allow the identification of storm events. The classification of the geostrophic wind direction, corresponds to an 8-point compass (N, NE, E, SE, S, SW, W, NW), a detailed description of the methodology and its application to the North Sea is given by Löwe et al. (2005). The Fig. 8 shows the frequency of easterly (50°-140°) and westerly (230°-320°) geostrophic North Sea winds for the period 1990–2011. In the German Bight these wind sectors are known for periods of persistent wind direction, which is a prior condition, that the local wind can shift the position and properties of fronts significantly. A total of 642 east wind and 2326 west wind days had been detected for this 20-year period.

The

Fig. 9 shows the monthly distribution of geostrophic east and west wind days for the period 1990–2011. As expected, both wind sectors show a different seasonal cycle. In a first approach, the distribution of the westerly winds has been adapted to that of easterly winds (

Fig. 9). However, thereby the seasonal dependency is not removed, because the effects of changing wind direction on the temporal statistics of fronts can be not distinguished from the effect of the seasonal temperature variations.

The observed distribution of all geostrophic wind direction in 1990–2011 is shown in Fig. 10. In order to remove the seasonal cycle of the wind distribution as far as possible, the wind distribution has been adjusted by selecting a uniform distribution regarding the months (Fig. 11). For the month August such an adaption was not

---

[4] http://www.cru.uea.ac.uk/cru/data/lwt/
[5] Reanalysis I, 1948 until present, Kalnay et al. (1996)

possible for of easterly winds due to a lack of satellite data and corresponding observations at this wind direction. In a random selection of satellite observations the conditions regarding to the cloud state is not defined, therefore the temporal statistics is influenced by a seasonal dependency again.

A further promising approach is the selection of the satellite scenes on pixel level and generating a uniform distribution with regard to the wind direction and the number of cloud-free observations. Due to time and budget restrictions this approach could not been realized in this project phase. In Fig. 12 we present some first results basing on the uniform distribution shown in Fig. 11. The Figures are based on AVHRR-sensor data of NOAA and MetOp satellites.
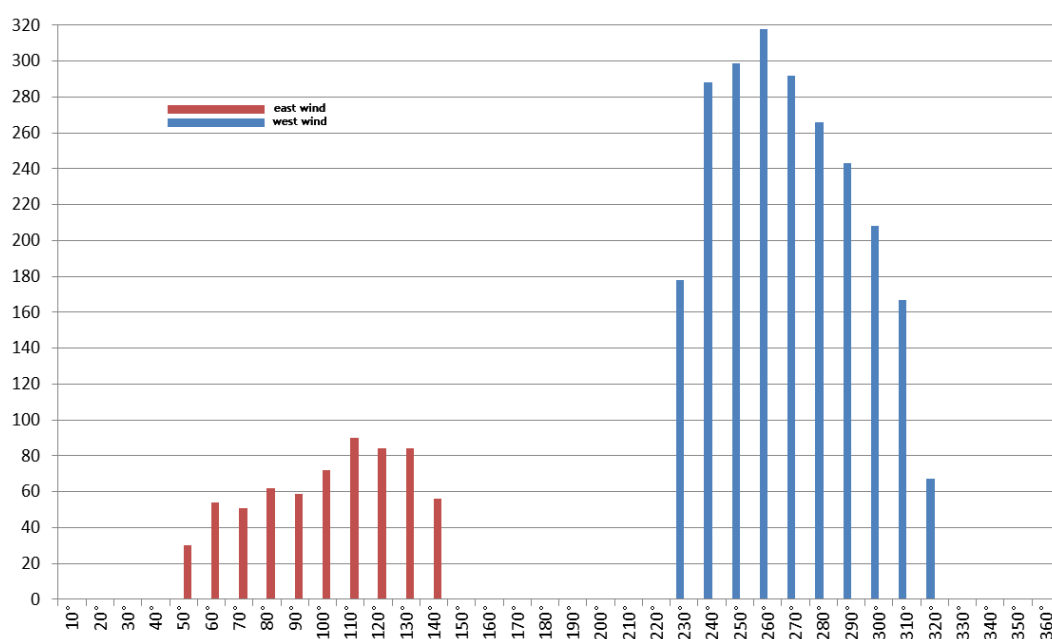

Fig. 8: Frequency of geostrophic east (red) and west (blue) winds over the North Sea. Daily means for 1990–2011.
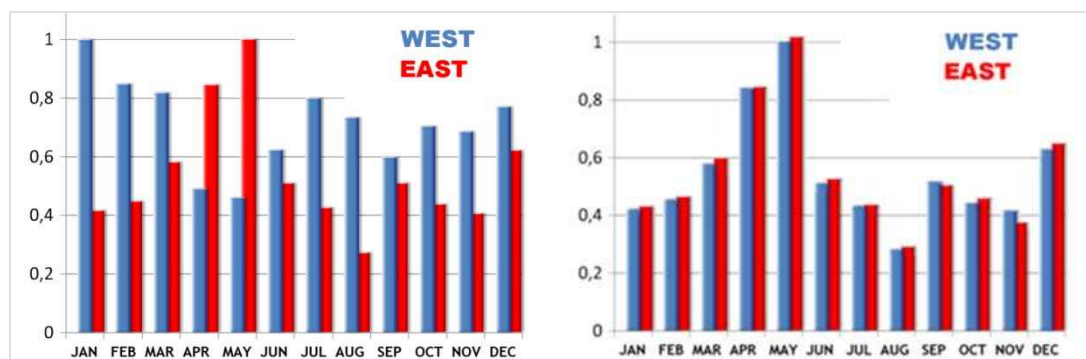

Fig. 9: Relative monthly frequency of geostrophic east (red) and west (red) winds wind direction. Daily means for 1990–2011. Left: original distribution, right: after adjusting the seasonal distribution of westerly winds to that of easterly winds.
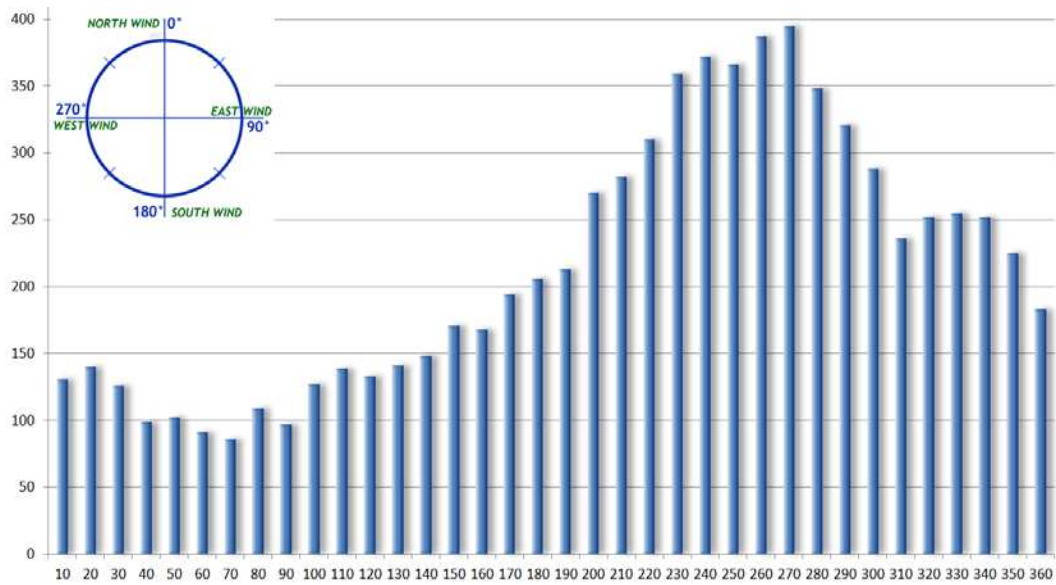
Fig. 10: Distribution of all geostrophic wind directions over the North Sea. Daily means for 1990–2011.
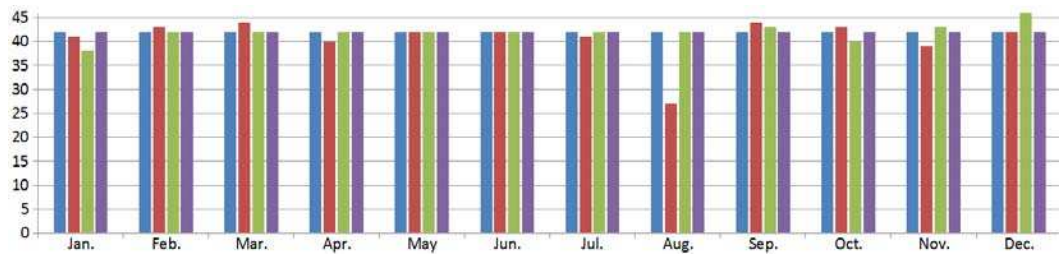

Fig. 11: Monthly frequency of the AVHHR products shown in Fig. 12. Red: east wind, blue: west wind, green: north wind, and violet: south wind.
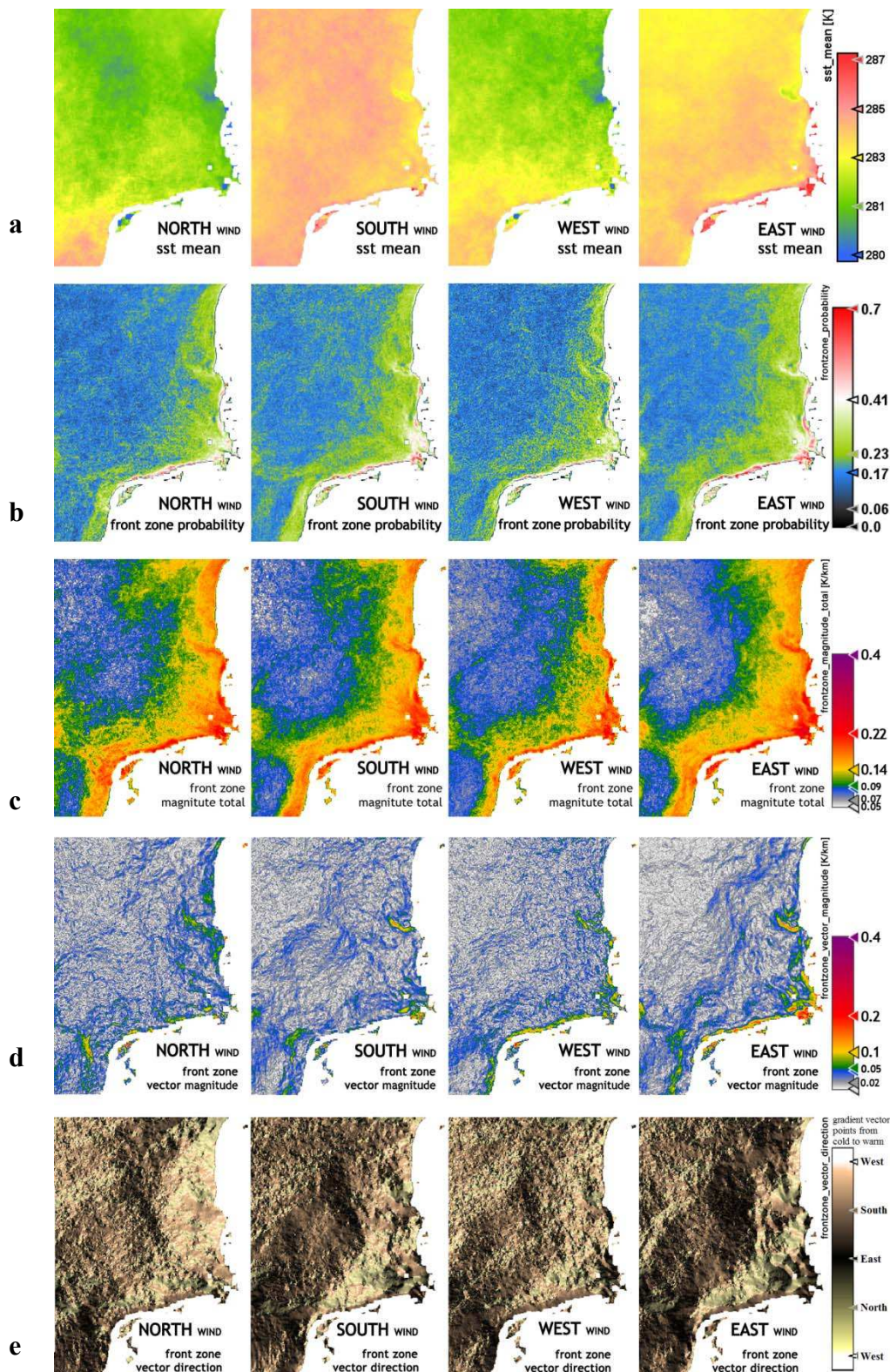
Fig. 12: Different front products based on the data of the AVHRR sensor on NOAA and MetOp from 1990-2011 for geostrophic wind from the north, south, west and east:
a: mean SST distribution, b: SST front probability, c: mean of gradient magnitude for SST frontal zone, d: magnitude of mean SST front gradient vector, and e: direction of mean SST front gradient vector.

Despite all restrictions discussed above, the preliminary products show clearly an impact of the wind field on front position and gradient strength. However, the results a basing on a large-scale wind field covering the whole North Sea which is not always representative for the German Bight or other selected area (see all the different meteorological forecast areas of European met services in the North Sea). Much more precise and significant results can be expected if the real local wind field (e.g. as recorded by station data) or hind-cast data are used for this analysis. Of course, this can't be done fully automatically, but should be added in a later project period for selected North Sea regions as an appendix for this climatology. First studies in the framework of KLIWAS have shown also, that frequency and local pattern of prevailing wind directions is expected to change over the North Sea in future decades (Gaslikova et al., 2012, Ganske and Rosenhagen, 2013). They suggest an increase of westerly directions and a decrease of northerly and easterly winds (Fig. 13) which will inevitable change the location and intensity of oceanic fronts.
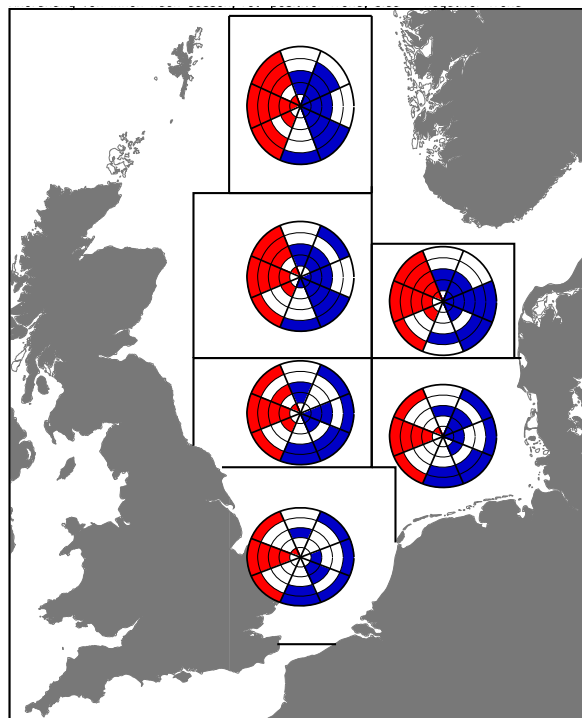

Fig. 13: Sign and significance of trends of yearly wind direction frequencies between 1961 and 2099 calculated with 5 different RCM runs for 5 North Sea subareas. Each segment of a circle shows the results for the corresponding wind direction class. Each circle contains the results of a specific RCM, where positive significant trends are shown in pink, negative significant trends in blue and non-significant trends in white. Shown are results from the runs of: IPSLCM/REMO, ECHAM5_1/REMO, MPI-OM/ECHAM5_3/REMO, ECHAM5_3/RACMO and ECHAM5_3/HIRHAM5 (from inner to outer circle). The figure shows the result for all wind speeds. By courtesy of A. Ganske.

6 Conclusions, Outlook and Summary

The new KLIWAS climatology of sea surface temperature (SST) and ocean colour (OC) fronts in the North Sea provides a reliable reference data set for the assessment of changes in frontal position, gradients, and seasonal variability due to climate change on the basis of satellite data. It is also a valuable addition to the new KLIWAS North Sea Climatology for oceanic and atmospheric in-situ data. The presented climatological data sets with annual, seasonal and monthly products clearly demonstrates that the GRADHIST algorithm can be used for SST as well as for OC data and can also be used with data from different sensors and from different oceanic areas.

The GRADHIST algorithm is based on a combination and modification of the gradient algorithm of Canny (1986) and the histogram algorithm of Cayula and Cornillon (1992). The main principles of both algorithms have been preserved and three significant improvements have been added: (1) the Scharr-Operator (Scharr 2004) for the computation of the gradient is used instead of the Sobel-Operator; (2) the use of an improved non-maximum suppression for optimising the fronts and finally (3) an iteration over different window sizes has been introduced when applying the histogram algorithm. The validation and testing of the new algorithm was carried out using both synthetic data as well as with case studies using real AATSR, AVHRR, MERIS and MODIS data (see Table 1). The GRADHIST technique provides the possibility to combine fronts derived from different sensors, however, the quality of the geo-location has to be taken into account, an aspect which is not discussed in the present paper.

Statistical measures likes probability of occurrence, mean front gradient magnitude as well as direction and magnitude of mean front gradient vector, allow for a quantitative determination of the frontal positions and gradient strength. It also allows for the determination of their natural variability, i.e., annual or seasonal cycles can be derived from the climatological data sets. Furthermore, a SST and OC fronts can be compared and potential relationships between both types of fronts can be analysed. During periods of strong solar radiation in spring or summer for instance, SST gradients can be strongly smoothed but a river plume front can still be tracked by the difference in TSM or yellow substance concentration between sea water and river run-off.

The compiled climatological data set demonstrates that the GRADHIST allows for an automated processing of comprehensive EO data volumes for front detection in the North Sea and other shelf sea areas. GRADHIST also enables the establishment of front maps as an operational downstream product which will help in monitoring potential change due to climate change or human impacts such as the installation of

large wind farms or off-shore structures. The operational use of the new method may also help in assuring the so-called Good Environmental Status (GES) as required by the European Marine Strategy Framework Directive as well as in the identification of vulnerable areas for marine spatial planning (The European Commission, 2010).

For Future applications there are several EO data sets which can be analysed by GRADHIST. The most promising sensor for the greater North Sea area will be the SLSTR and OLCI on Sentinel-3 which will provide SST and OC data with a spatial resolution of 300 m. First data are expected to be available in 2015. The Group for High Resolution SST (GHRSST) provides several ultra-high resolution (UHR, <5km resolution) regional SST products, however, up to now they are excluding the North Sea area (GHRSST, 2009). The AVHRR SST Pathfinder Project Version 5.2 reprocessed the entire 1981-2009 archive at the 4 km Global Area Coverage (GAC) level, the highest resolution globally achievable. This data is now available, but not useful for front detection in the North Sea due to its spatial resolution. However, for Version 6 they planned a large collection of High-Resolution Picture Transmission (HRPT) and Local Area Coverage (LAC) data collected at stations around the world. The HRPT or LAC data at roughly 1.1 km resolution are applicable for the front detection and for analysis of the time series (Casey et al. 2010).

An important analysis to be added in the future is the impact of the local wind field on frontal position and gradient strength. The analysis presented in Chapter 5 with a mean geostrophic wind field for the whole North Sea area should be repeated for selected areas with local wind fields. Especially the RPFs in coastal waters are known to be influenced by selected wind directions if they are persisting for a few days to allow the fronts to adjust to the wind field. Another aspect not mentioned up to now is the influence of changing river run-offs into the North Sea due to changing precipitation patterns and volumes over land on RPFs. However, also these changes can be detected and monitored by GRADHIST on the basis of the new climatology.

7   Data Access

7.1 Data format and access

The data format used is netcdf (netcdf 3, cf-conform).

The data are hosted on a server of the company Brockmann Consult. It is required to register by email to get access to this dataset:

fronten@brockmann-consult.de

Following information is needed and has to be included within your e-mail for granting access.[6]

- First name and last name
- Email address
- Organization
- How do you intend to use this dataset?

7.2 Structure of Data

Structure of folders:

- Sensor
    - time period
    - time period - season
    - time period - months (if available)

Structure of products:

- Bands
    - Bathymetry
    - Land/water mask
    - Number of observations
    - Number of front observation
    - Front probability
    - Mean of gradient magnitude for frontal zone
    - Front gradient vector
        - magnitude of mean front gradient vector
        - direction of mean front gradient vector

---

[6] Brockmann Consult GmbH does not and will not share any of this information with anyone outside of our institution, except as required to comply with all relevant state and federal laws.

8 Acknowledgement

9 References

Amante, C. and B.W. Eakins 2009: ETOPO1 1 Arc-Minute Global Relief Model: Procedures, Data Sources and Analysis. NOAA Technical Memorandum NESDIS NGDC-24, 19pp

Belkin, I.M. and J.E. O'Reilly 2009: An algorithm for oceanic front detection in chlorophyll and SST satellite imagery. Journal of Marine Systems 78, 319–326

Campbell, J.W. 1995: The lognormal distribution as a model for bio-optical variability in the sea. Journal of Geophysical Research 100 (C7), 13237–13254

Canny, J.F 1986: A computational approach to edge detection. IEEE Transactions on Pattern Analysis and Machine Intelligence 8(6), 679–698

Castelao, R.M., T.P. Mavor, J.A. Barth and L.C. Breaker 2006: Sea surface temperature fronts in the California Current System from geostationary satellite observations. Journal of Geophysical Research 111(C09026), 1-13

Cayula J.-F. and P. Cornillon 1992: Edge detection algorithm for SST images. Journal of Atmospheric and Oceanic Technology 9(1), 67–80

Cayula J.-F. and P. Cornillon 1995: Multi-image edge detection for SST images. Journal of Atmospheric and Oceanic Technology, 12, 821–829

Cayula J.-F. and P. Cornillon 1996: Cloud detection from a sequence of SST images. Remote Sensing of Environment 55, 80–88

Diehl S. F., J.W. Budd, D. Ullman and J.-F. Cayula 2002: Geographic Window Sizes Applied to Remote Sensing Sea Surface Temperature. Journal of Atmospheric and Oceanic Technology 19, 1105–1113

Doerffer R. and H. Schiller H. 2008: Algorithm Theoretical Basis Document (ATBD) - MERIS - Lake Water Algorithm for BEAM, GKSS Forschungszentrum Geesthacht GmbH

Ferrari, R. 2011: A frontal challenge for climate models. Science, 332, 316-317

Fisher, R., S. Perkins, A. Walker and E. Wolfart 2003: Hypermedia Image Processing Reference (HIPR2). http://homepages.inf.ed.ac.uk/rbf/HIPR2/hipr_top.htm (accessed 2013/06/01)

Ganske, A. and G. Rosenhagen 2013: Wind Speed and Direction over the North Sea from Climate Model Results. In preparation

Gaslikova, L., I. Grabemann and N. Groll 2012: Changes in North Sea storm surge conditions for four transient future climate realizations.*Nat. Hazards,* Volume 66, Issue 3 , pp 1501-1518

Gregg, W.W. and N.W. Casey 2004: Global and regional evaluation of the SeaWiFS chlorophyll data set. Remote Sensing of Environment 93 (4), 463–479

GHRSST (2009). http://www.ghrsst.org/

ICES 2006: Report of the workshop on the indices of mesoscale structures (WKISMS), 22–24 February 2006, Nantes, France. International Council for the Exploration of the Sea, WKIMS Report 2006, 48pp

Jähne, B. 2005: Digitale Bildverarbeitung, Springer Verlag, 6th edition

Jenkinson, A. and F. Collison 1977: An initial climatology of gales over the North Sea. Synoptic Climatology Branch Memorandum, No. 62, UK Met Office, Bracknell, 18pp

Kalanay, E., M. Kanamitsu, R. Kistler, W. Collins, D. Deaven, L. Gandin, M. Irdell, S. Saha, G. White, J. Woollen, Y. Zhu, M. Chelliah, W. Ebisuzaki, W. Higgins, J. Janowiak, K. C. Mo, C. Ropelewski, J. Wang, Y. A. Leetmaa, R. Reynolds, R. Jenne, D. Joseph 1996: The NCEP/NCAR 40-Year Reanalysis Project. Bull. Amer. Meteor. Soc.,77, 437-471

Kirches, G., M. Paperin, H. Klein, K. Stelzer and C. Brockmann 2013: Detection and Analysis of Fronts in the North Sea. In:Proceedings of the Sentinel-3 OLCI/SLSTR and MERIS/(A)ATSR Workshop - 15–19 October 2012 Frascati, Italy, SP-711, January 2013, ISBN 978-92-9092-275-9

Löwe, P. (Ed.), S. Schmolke, G. Becker, U. Brockmann, S. Dick, C. Engelke, A. Frohse, W. Horn, H. Klein, S. Müller-Navarra, H. Nies, N. Schmelzer, D. Schrader, A. Schulz, N. Theobald und S. Weigelt 2005: Nordseezustand 2003. Berichte des Bundesamtes für Seeschifffahrt und Hydrographie, Nr. 38, 217pp

Miller, P.I. 2009: Composite front maps for improved visibility of dynamic sea-surface features on cloudy SeaWiFS and AVHRR data. Journal of Marine Systems 78 (3), 327–336

Ocean Color 2009: Ocean Color Data Product Documents, http://oceancolor.gsfc.nasa.gov/DOCS/ocformats.html

Rutherford Appelton Laboratory- RAL 2007: The ATSR Project, http://www.atsr.rl.ac.uk/index.shtml

Scarpino M.G., M. Cardaci and S. Procter 2009: ENVISAT-1 Products Specifications, Volume 7: AATSR Products Specifications, ESA Doc Ref :PO-RS-MDA-GS-2009

Scharr, H. 2000: Optimal Operators in Digital Image Processing - Dissertation (PhD thesis), Interdisciplinary Center for Scientific Computing, Ruprecht-Karls-Universität Heidelberg, Germany

Shimada, T., F. Sakaida, H. Kawamura and T. Okumura 2005: Application of an edge detection method to satellite images for distinguishing sea surface temperature fronts near the Japanese coast, Remote Sensing of Environment 98(1), 21-34

The European Commission 2010: On criteria and methodological standards on good environmental status of marine waters. Official Journal of the European Union 2.9.2010, L 232/14, 11pp

Thomas, H., Y. Bozec, K. Elkalay and H.J.W. de Baar, 2004: Enhanced open ocean storage of CO_2 from shelf sea pumping. Science, 304, 1005-1008.

Ullman, D.S. and P.C. Cornillon 1999: Satellite-derived Surface temperature fronts off the East Coast of North America from AVHRR imagery. Journal of Geophysical Research 104(C10), 23459-23478

Ullman, D.S. and P.C. Cornillon 2000: Evaluation of front detection methods for satellite-derived SST data using in situ observations. Journal of Atmospheric and Oceanic Technology 17, 1667-1675

Ullman, D.S. and P.C. Cornillon 2001: Continental shelf surface thermal fronts in winter off the northeast US coast. Continental Shelf Research 21, 1139-1156

Vazquez, D.P., C. Atae-Allah and P.L. Luque-Escamilla 1999: Entropic approach to edge detection for SST images, Journal of Atmospheric and Oceanic Technology 16(7), 970-979

Bundesanstalt für Wasserbau
Kompetenz für die Wasserstraßen

Bundesanstalt für Wasserbau (BAW)

Kußmaulstraße 17
76187 Karlsruhe

www.baw.de
info@baw.de

Bundesamt für Seeschifffahrt und Hydrographie (BSH)

Bernhard-Nocht-Straße 78
20359 Hamburg

www.bsh.de
posteingang@bsh.de

BUNDESAMT FÜR SEESCHIFFFAHRT UND HYDROGRAPHIE

Deutscher Wetterdienst (DWD)

Frankfurter Straße 135
63067 Offenbach/Main

www.dwd.de
info@dwd.de

Bundesanstalt für Gewässerkunde (BfG)

Am Mainzer Tor 1
56068 Koblenz

www.bafg.de
posteingang@bafg.de

bfg Bundesanstalt für Gewässerkunde